Agricultural and Forest Meteorology 252 (2018) 296–310

Contents lists available at ScienceDirect

Agricultural and Forest Meteorology

journal homepage: www.elsevier.com/locate/agrformet

Evapotranspiration partitioning for three agro-ecosystems with contrasting moisture conditions: a comparison of an isotope method and a two-source model calculation

Zhongwang Wei[a,b,*], Xuhui Lee[a,b,*], Xuefa Wen[c], Wei Xiao[a]

[a] Yale-NUIST Center on Atmospheric Environment, Nanjing University of Information Science & Technology, Nanjing, Jiangsu, China
[b] School of Forestry and Environmental Studies, Yale University, New Haven, CT, USA
[c] Key Laboratory of Ecosystem Network Observation and Modeling, Institute of Geographic Sciences and Natural Resources Research, Chinese Academy of Sciences, Beijing, China

ARTICLE INFO

Keywords:
Agro-ecosystems
Evapotranspiration partitioning
Isotope
Two-source model

ABSTRACT

Quantification of the contribution of transpiration (T) to evapotranspiration (ET) is a requirement for understanding changes in carbon assimilation and water cycling in a changing environment. So far, few studies have examined seasonal variability of T/ET and compared different ET partitioning methods under natural conditions across diverse agro-ecosystems. In this study, we apply a two-source model to partition ET for three agro-ecosystems (rice, wheat and corn). The model is coupled with a plant physiology scheme for the canopy conductance. The model-estimated T/ET ranges from 0 to 1, with a near continuous increase over time in the early growing season when leaf area index (LAI) is less than 2.5 and then convergence towards a stable value beyond LAI of 2.5. The seasonal change in T/ET can be described well as a function of LAI, implying that LAI is a first-order factor affecting ET partitioning. Application of the model to seven other Ameriflux sites reveals that soil moisture and canopy conductance also influence the ET partitioning. The two-source model results show that the growing-season (May–September for rice, April–June for wheat and June–September for corn) T/ET is 0.50, 0.84 and 0.64, while an isotopic approach shows that T/ET is 0.74, 0.93 and 0.81 for rice, wheat and maize, respectively. The two-source model results are supported by soil lysimeter and eddy covariance measurements made during the same time period for wheat (0.87). Uncertainty analysis suggests that further improvements to the Craig-Gordon model prediction of the evaporation isotope composition and to measurement of the isotopic composition of ET are necessary to achieve accurate flux partitioning at the ecosystem scale using water isotopes as tracers.

The program code for the two-source model is available at the open-source platform https://github.com/zhongwangwei/SiLSM_v3.

1. Introduction

Evapotranspiration (ET), a combination of soil or substrate evaporation (E) and plant transpiration (T), is an essential component of the terrestrial water cycle. Knowledge about the contribution of T to ET is important for understanding changes in carbon assimilation and in water cycling in a changing environment, and has received intensive attention from the scientific community in recent years (Jasechko et al., 2013; Good et al., 2015; Maxwell and Condon, 2016; Miralles et al., 2016; Wei et al., 2017). Traditionally, the transpiration fraction T/ET can be determined by combining in-situ measurements, including eddy covariance systems (Baldocchi and Meyers, 1991; Wilson et al., 2001; Agam et al., 2012), Bowen ratio equipment (Ashktorab et al.,1989; Zeggaf et al., 2008; Holland et al., 2013), weighing lysimeters (Boast and Robertson, 1982; Shawcroft and Gardner, 1983; Walker, 1984; Zhang et al., 2002), sap flow meters (Sakuratani, 1981, 1987; Williams et al., 2004), up-scaling of leaf (Kato et al., 2004; Ding et al., 2014) and soil chamber measurements (Stannard and Weltz, 2006; Rothfuss et al., 2010; Raz-Yaseef et al., 2012), and isotopic labeling (Wang and Yakir, 2000; Williams et al., 2004; Yepez et al., 2005; Hu et al., 2014; Good et al., 2014). Only a few studies have investigated drivers of seasonal variability of T/ET (Liu et al., 2002; Raz-Yaseef et al., 2012; Wang et al., 2015; Wei et al., 2015) and the issue about how different partitioning techniques compare with each other across diverse ecosystems and soil moisture conditions (Wilson et al., 2001; Moran et al., 2009; Wang et al., 2015).

* Corresponding authors at: School of Forestry and Environmental Studies, Yale University, New Haven, CT, USA.
E-mail addresses: zhongwang.wei@yale.edu (Z. Wei), xuhui.lee@yale.edu (X. Lee).

https://doi.org/10.1016/j.agrformet.2018.01.019
Received 17 February 2017; Received in revised form 10 January 2018; Accepted 15 January 2018

ET partitioning is also a subject of modeling investigation. A frequently-used model is that proposed by Shuttleworth and Wallace (1985); hereafter S-W model). In this model, the energy balance constraint is applied separately to the soil and the canopy of sparse natural ecosystems and heterogeneous crops to calculate water and heat transfers from these two sources (e.g. Vörösmarty et al., 1998; Stannard, 1993; Kato et al., 2004; Hu et al., 2009; Ding et al., 2014). A large uncertainty of the S-W model is related to the determination of canopy resistance (r_{sc}) because the model is very sensitive to r_{sc}. Typically, r_{sc} is calculated by scaling up leaf stomatal resistance using the Jarvis-Stewart parameterization (e.g. Hu et al., 2009; Kato et al., 2004). It is known that the Jarvis-Stewart functional parameters calibrated for a local environment do not necessarily work in future climates with elevated carbon dioxide concentrations or at a different site where environmental conditions are different from those of the calibration site (Ronda et al., 2001). Alternatively, r_{sc} can be parameterized according to plant physiological constraints (the Ball-Berry-Collatz type). Parameterizations of the Ball-Berry-Collatz type have gained widespread use in land surface schemes (e. g. Cox et al., 1998, Sellers et al., 1996). Different from the Jarvis-Stewart parameterization, the canopy conductance in the Ball-Berry-Collatz parameterization is an indirect function of the environmental variables evaluated at the leaf level and is linearly related to the gross assimilation rate. Thus, it directly links the terrestrial water flux with the carbon flux and is more appropriate for prognostic atmospheric models and climate impact studies (e.g. Cox et al., 2000; Medvigy et al., 2010). One such physiological parameterization has been developed by Ronda et al. (2001), which includes an analytical expression that links r_{sc}, a canopy-scale property, to leaf-scale photosynthetic capacity so that the effects of soil moisture, solar radiation, and vapor pressure deficit are accounted for. Although this r_{sc} model has been successfully implemented in various modeling frameworks, such as large eddy simulations (Lee et al., 2011), mesoscale weather forecast models (e.g. Niyogi et al., 2009) and in offline site diagnostic analyses (e.g. Egea et al., 2011), it has not yet been incorporated into the S-W model.

Stable water isotope is a natural tracer of ecosystem processes and a useful tool for partitioning evapotranspiration at the ecosystem scale. To apply this method, detailed knowledge of isotopic fractionation in the different phases of water in the soil, the vegetation, and the atmosphere is required. Historically, because of difficulties in measuring the isotopic compositions of water vapor samples, very few studies have reported successful implementation of long-term (weeks to a season) isotopic partitioning. Recently, laser spectroscopy technology allows measurement of water vapor isotopic ratios at a high temporal resolution and on a continuous basis (Lee et al., 2006; Wei et al., 2015). Such measurements reveal quantitative information on temporal variations of water vapor isotopic ratios and the mechanisms involved. Thus, isotope-based ET partitioning studies have been increasing in recent years (e.g. Rothfuss et al., 2010; Dubbert et al., 2014a; Good et al., 2014; Hu et al., 2014; Wen et al., 2016; Wei et al., 2015; Berkelhammer et al., 2016; Wang et al., 2016).

The isotopic method still faces several challenges. A successful ET partitioning requires that all the three isotopic endmembers, the isotopic composition of transpiration (δ_T), soil evaporation (δ_E) and evapotranspiration (δ_{ET}) be known accurately. Recent studies have raised doubt about the steady state assumption (SSA) that δ_T is equal to the isotopic composition of the xylem water (e.g. Lai et al. 2006; Lee et al., 2007; Dubbert et al., 2014a; Dubbert et al., 2014b; Hu et al., 2014; Wang et al., 2015). These studies show that δ_T is in non-steady state (NSS), deviating from the isotopic composition of the xylem or source water, through the diurnal time scale. Moreover, the assumptions underlying δ_{ET} (such as the Keeling plot) and δ_E (such as determination of the δ_E source using a measurement at an assigned soil depth) estimation may not hold under field conditions (Dubbert et al., 2013; Lee et al., 2006; Werner et al., 2012). Little is known about the impact of these challenges on long-term (weeks or longer) ET partitioning.

Stable water isotopes have also been incorporated as tracers into land surface models to better understand energy and water fluxes (Riley et al., 2003; Henderson-Sellers et al., 2006; Yoshimura et al., 2008; Xiao et al., 2010; Cai et al., 2015; Wang et al., 2015). These studies demonstrate that an isotope-enabled ET model is a useful tool to address the dynamics that drive temporal and seasonal variability of T/ET and to understand whether the different techniques agree under natural conditions across diverse ecosystems. However, it is challenging to integrate processes underlying the dynamic variations in the plant transpiration and soil evaporation fluxes and those underlying isotopic fractionation of these fluxes, in large part because of the lack of high resolution field observations and the difficulty of undertaking targeted *in-situ* water vapor isotope measurements (Riley et al., 2003; Cai et al., 2015; Wang et al., 2015).

Rice, corn and wheat are staple crops providing the dominant diet of the global human population. Their cultivation costs more than half of the irrigation water consumption in the world (Siebert and Döll, 2010). As agricultural areas expand over time to meet the increasing demand for food, a better understanding of water loss through transpiration relative to that lost through evaporation is necessary for improving water resource management. Moreover, since climate change impacts on soil moisture will lead to significant changes on soil evaporation and plant transpiration, it is crucial to develop a crop model capable of simulating crop water usage in response to environmental changes. In this study, we investigate the contributions of evaporation and transpiration to ET by utilizing near-continuous ecosystem-scale isotope and eddy covariance measurements for these three crops. Specifically, the objectives of the present study are as follows: (1) to develop an isotope-enabled two-source model, by coupled energy balance constraints with a plant physiology approach provided by Ronda et al. (2001) to calculate the canopy conductance and with the non-steady state isotopic fractionation mechanism of transpiration described by Farquhar and Cernusak (2005); (2) to investigate the dynamics that drive daily variabilities of T/ET in the three crop ecosystems; (3) to perform model sensitivity analyses to explore potential uncertainties in model parameterizations and to identify variables that exert large controls on ET partitioning; and (4) to compare the relative strengths of different approaches (lysimeter based, two-source model, and isotope-based) for quantifying T/ET.

2. Methods

2.1. Study sites

During the growing season in 2014, field observations were conducted at a rectangular experimental rice paddy field in Mase, Tsukuba, Japan (36° 03′ N, 140° 01′ E, elevation 12 m above the mean sea level). Around the site, a field of about 150 ha was used exclusively for planting rice (Oryza sativa L; Wei et al., 2016). The mean annual precipitation and air temperature were approximately 1200 mm and 13.7 °C, respectively. Irrigation started on 24 April, 2014. Rice was sown on 2 May and was harvested at the end of August. The soil texture of the paddy fields is clay loam. During the full growing season, the field was flooded to a mean water depth of 3.0 cm. Periodic measurements of leaf area index (LAI) are plotted in Fig. 1.

The other experiment was conducted at the Luancheng Agro-Ecosystem Experimental Station (37° 53′ N, 114° 41′ E), located in the North China Plain, which is a major agricultural region in China (Wen et al., 2012; Xiao et al., 2012). A field study was conducted in a winter wheat and summer corn rotation. Wheat (Triticum aestivum L.) was planted in November of 2007 and harvested on June 18, 2008, with a maximum LAI of 4.5 (Fig. 1) and a maximum height of 0.75 m. Corn (Zea mays L.) was planted at the beginning of June before wheat harvest and was harvested in mid-September. The corn canopy reached a maximum LAI of 4.2 and a maximum height of 2.77 m on August 16 (Fig. 1). The site is controlled by a semi-arid monsoonal climate, with a

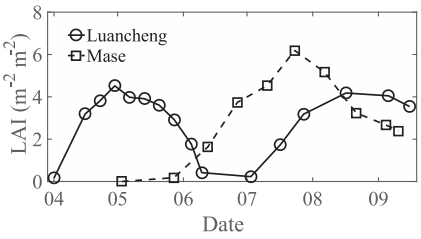

Fig. 1. Seasonal variations of leaf area index (LAI).

mean annual precipitation of 480 mm and a mean annual temperature of 12.2 °C (Sun et al., 2006). Soil moisture field capacity is approximately 34% by volume in the top 100 cm soil layer (Sun et al., 2006).

2.2. Observation systems

2.2.1. Meteorological measurements

At the Mase site, an eddy covariance system, consisting of an open-path, non-dispersive infrared gas analyzer (LI-7500, Li-cor., Lincoln, NB, USA) and a 3D ultrasonic anemometer (DA-600, Kaijo., KAIJO Corp., Japan) mounted at a height of 3.0 m above the ground was used to measure momentum, sensible heat and latent heat fluxes. Air temperature (Ta) and relative humidity (RH) were measured by two temperature-humidity sensors (HMP-45A, Vaisala Helsinki, Finland) at two heights (1.1 and 3.8 m) above the ground. Radiation flux densities were measured at a height of 2.3 m above the ground using a four-component net radiometer (CNR1, Kipp & Zonen, The Netherlands). Wind direction and wind speed were measured by a vane (VF016, Makino Applied Instruments, Tokyo, Japan) and a cup anemometer (AF-750, Makino, Tokyo, Japan) at a height of 4.3 m. Because the ground was flooded, the total conduction heat flux (into the water column and the soil) was calculated from the heat storage in the standing water and the heat flux in the soil. Soil heat fluxes were measured by thermopile-type heat flux plates (MF-180M; Eko, Japan) at 0–2.5 cm, 0–5 cm, 0–10 cm, 0–20 cm and 0–30 cm below the soil surface. Mean water temperature was measured by a T-type thermocouple and the heat storage in the water was estimated from water depth and the time rate of change of the water temperature. The data collected in the 2014 season was used in this study.

At the Luancheng site, the experiment took place in 2008. The eddy fluxes of momentum, latent heat and sensible heat were measured using a sonic anemometer (CSAT-3; Campbell Scientific Inc.) and a CO_2/H_2O infrared analyzer (LI-7500; Licor Inc., Lincoln, NB, USA), which were mounted at a 3 m height above the ground. Soil temperature was measured using thermocouples (105T; Campbell Scientific Inc.) at three depths (10, 20, and 50 cm) below the surface. Soil heat flux was measured with three ground heat flux sensors (HFP01; Campbell Scientific Inc.) at a depth of 2 cm. No calorimetric correction made for 0–2 cm depth. Auxiliary measurements included Ta and RH (HMP45C; Campbell Scientific Inc.), and wind speed (A100R; Vector Instruments, Rhyl, North Wales, UK) at 1.4 m and 3.9 m heights above the ground. Net radiation (Rn) was measured with a 4-component radiometer (CNR-1; Kipp & Zone, Delft, The Netherlands). Water content reflectometers (CS616-L; Campbell Scientific Inc.) were used to measure the soil water content (θ_s) at 5, 20, and 50 cm depths. Precipitation was measured by a rain gauge (TE525MM; Campbell Scientific Inc.). Soil evaporation was measured with 2 small weighing lysimeters (120 mm diameter, 200 mm depth) placed between two rows during the later part of the wheat growing season. The micro-lysimeters contained isolated bare soil columns, and were mounted flush with the soil surface, and were weighed daily to determine water loss using an electronic balance with 0.001 kg precision (Liu et al., 2002). The soil in the lysemeters was changed once per day to every couple of days to keep the soil moisture in micro-lysimeters in agreement with that between the rows. The ratio of daily canopy transpiration over evapotranspiration were then calculated as T/ET = 1- E/ET.

Energy imbalance was observed at these study sites (about 22% at Mase and 10% at Luancheng). Since the S-W model is based on the principle of energy budget conservation, we assume that the energy imbalance was caused by eddy covariance measurement biases. For model performance evaluation, we adjusted measured half-hourly latent heat flux (LE) and sensible heat flux (H) by an adjustment factor derived from the Bowen ratio (H/LE), to achieve energy balance closure with the assumption that the Bowen ratio was measured accurately (Twine et al., 2000; Blanken et al., 1998).

2.2.2. Isotope measurements

All isotope measurements are presented as the ratio of heavy [^{18}O (H_2O)] to light [$^{16}O(H_2O)$] isotopologues and are relative to the normalized delta notation in per mil (‰). The reference standard is VSMOW. A water vapor isotopic measurement system at the Mase site consisted of a cavity ring-down spectrometer (model L2120-i), a standard delivery module (A0101), a high-precision vaporizer (A0211), and a 16-port distribution manifold (A0311; Picarro, Sunnyvale, CA, USA; Wei et al., 2015). Air was drawn from a height of 2 m above the ground to the spectrometer, which was calibrated with the standard delivery module. The isotopic measurement was made at 1 Hz and was averaged to 30 min intervals. The high frequency (1 Hz) measurement was used in a Keeling mixing line analysis to determine the isotopic composition of ET. Surface standing water in the rice paddy was sampled 3 days per week. The liquid water samples were analyzed using another cavity ring-down spectrometer (L2120-i) in the laboratory. Detailed information can be found in Wei et al. (2015) and Wei et al. (2016).

At the Luancheng site, the O^{18}/O^{16} ratio in water vapor was measured continuously using a tunable diode laser trace gas analyzer (Model TGA100A; Campbell Scientific Inc., Utah, USA; Wen et al., 2012). Water vapor was sampled at two heights above the canopy which were adjusted according to plant growth. The isotopic composition of evapotranspiration was determined from the gradient measurement using the flux-gradient relationship (Lee et al. 2006). Soil samples were collected from 3 different depths (0–5, 15–20 and 40–45 cm). Leaf, stem and soil samples were collected from four sampling plots within 50 m of the gas intakes every 2–4 days. The main leaf vein was removed from leaf samples and the upper and lower canopy were archived separately. Liquid water in the soil, leaf and stem samples was extracted using a vacuum extraction system and isotopic measurements were made with an isotopic ratio infrared spectroscopy (DLT-100; LGR, CA, USA). Interference by organic containments was corrected following the procedure of Schultz et al. (2011). Detailed information can be found in Wen et al. (2012) and Xiao et al. (2012).

2.3. Model description

2.3.1. Shuttleworth-Wallace model

The overall model structure is shown in Fig. 2. Briefly, the S-W model is a variation of the Penman-Monteith model constrained by energy conservation. It simulates the soil evaporation and canopy transpiration in hourly time resolution. The model takes into consideration the different resistances encountered by soil evaporation and canopy transpiration. In this study, the S-W model was coupled with a photosynthesis-stomatal (g_s-A_c) conductance sub-model developed by Ronda et al. (2001) to calculate the canopy transpiration. Mathematical details of the S-W model and the photosynthesis-stomatal conductance sub-model are presented in Appendix A. The g_s-A_c model is a plant physiological approach which makes a distinction between C3 and C4 plant types. Different parameterizations used for the biochemical module of C3 (rice and wheat) and C4 (corn), including the mesophyll conductance, the initial light use efficiency, the CO_2 compensation point and the maximal primary productivity, are presented in Table A1 of Ronda et al. (2001). At the Luancheng site (wheat and corn), the influence of soil moisture stress on the canopy conductance was evaluated using a quadratic stress function (Appendix A). At the Mase site,

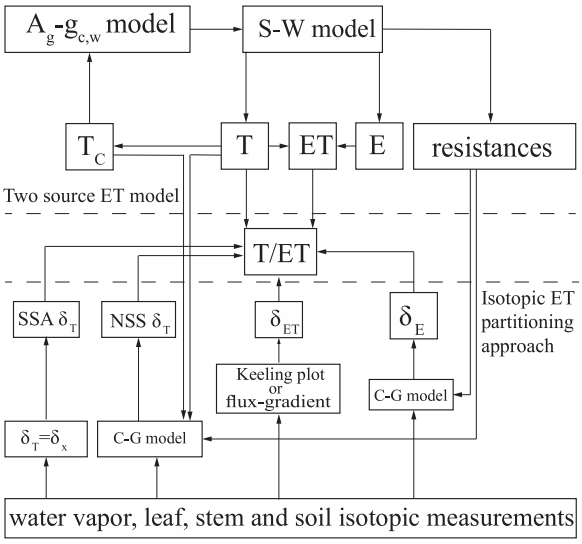

Fig. 2. Schematic representation of the two source-model and its relationship to the isotopic tracer method. S-W: Shuttleworth and Wallace model; SSA: steady state isotopic behavior of transpiration; NSS: non-steady state isotopic behavior; C-G: Craig-Gordon model: A_g-$g_{c,w}$: canopy resistance model developed by Ronda et al. (2001).

because there was no soil moisture stress, the quadratic stress function value was assigned a value of one.

The input data of the S-W model included air temperature, relative humidity, net radiation, wind speed, atmospheric CO_2 concentration, air pressure, soil temperature and moisture, LAI, and canopy height. The tunable parameter in the stomatal parameterization, the vapor pressure deficit constant D0 in Eq. (11) of Ronda et al. (2001), was determined by minimizing the root mean square error (RMSE) between the simulated and the observed latent heat flux. The optimization results were D0 = 0.245 kPa for rice, D0 = 0.250 kPa for wheat and D0 = 0.160 kPa for corn, respectively (Supplementary Table S1). It is noted that our stomatal parameterization is different from that in the big-leaf model proposed by Xiao et al. (2010) and applied to the same experiment at Luancheng (Xiao et al. 2012). The study by Xiao et al. (2012) aims to investigate temporal variability of foliage isotope compositions. The version used by Xiao et al. contains two tunable parameters: D0 and the CO_2 concentration constant a1, where D0 = 0.50 kPa and a_1 = 11.9 for wheat and D0 = 0.74 kPa and a1 = 4.2 for corn were determined by a nonlinear least squares method to minimize the difference between the observed and the simulated latent heat flux. The present study adopted the original a1 parameter values in Ronda et al. (2001) (a1 = 9.1 for C3 and 6.6 for C4 plants). The canopy temperature (T_c) used by the g_s-A_c sub-model (Fig. 2) was solved iteratively until a stable value was reached.

Soil surface resistance (r_{ss}) is calculated as a function of soil moisture content (Sellers et al., 1992; Appendix B).

Validation was performed against the eddy covariance ET measurements. The model calibration ensures that ET is unbiased but it does not guarantee that the total water vapor flux is partitioned properly. The ET partition may be sensitive to how the net radiation is divided between the canopy and the substrate (Eq. A11) and to the soil surface resistance parameterization (Eq. A18). A Monte Carlo analysis was performed to quantify this error propagation. In this analysis, a total of 1000 ensemble members were calculated, with errors in the light extinction coefficient (k_r, Eq. A11) and the two coefficients in Eq. A18 following a normal distribution with standard deviations of 10% of the original value.

To investigate the relationship of T/ET with LAI, soil moisture and canopy resistance, we also applied to the S-W model to 7 AmeriFlux crop sites, bringing the total number of sites to 10 (Supplementary Table S1). Of these, 7 were irrigated (Luancheng Wheat, Luancheng Corn, Maze Rice, US-NE1 Soybean, US-NE1 Corn, US-NE2 Soybean and US-NE2 Corn) and 3 were rain-fed (US-NE3 Soybean, US-NE3 Corn and US-RO3). Except for the vapor pressure deficit constant D0 (Supplementary Table S1), all other parameters in the model were unchanged. We chose these AmeriFlux sites because the soil moisture and LAI data were available at sufficient time resolutions to drive the model simulation.

2.3.2. Isotopic partitioning approach

The isotope partitioning approach is based on mass balance consideration for both the major and the minor isotopologues. Utilizing a two end-member (E and T) mixing model, the partitioning can be expressed as

$$T/ET = \frac{\delta_{ET} - \delta_E}{\delta_T - \delta_E} \quad (1)$$

(Yakir and Sternberg, 2000). This equation requires that the isotopic ratio of the ET, E and T fluxes be known from direct measurement or model estimation. In this study, δ_{ET} at the Mase site was determined from the vapor isotope measurement using the Keeling plot approach, and δ_{ET} at the Luancheng site was measured with the flux-gradient method.

The isotopic composition of substrate evaporation (δ_E) was calculated with the Craig and Gordon (hereafter C-G) model (Craig and Gordon, 1965; Appendix C). Input variables of the C-G model included the isotopic ratios of vapor (δ_v) measured at the reference height above the canopy and soil (in the case of Luancheng) or surface (in the case of Mase) water (δ_s), air temperatures, soil or surface water temperature, relative humidity, and the kinetic fractionation associated with substrate evaporation (ε_k). Different ε_k values were applied to the two sites to account for the fact that substrate evaporation originated from two different media (soil in Luangcheng and standing water in Mase; Appendix C): A constant ε_k value of 21‰ based on the chamber evaporation study of Kim and Lee (2011) was used for Mase and the parameterization of Wen et al. (2012) was used for Luancheng.

The isotopic composition of transpiration (δ_T) was estimated under two different assumptions. Under the steady-state assumption (SSA), δ_T was assumed to be the same as the delta value of stem water. Under the condition of non-steady state (NSS) isotopic behavior of transpiration, δ_T is also affected by temporal changes in foliage water content (W) and the transpiration rate (T). To determine δ_T in non-steady state, the model proposed by Farquhar and Cernusak (2005), accounting for the change in the water content and the Péclet effect, was used. The measured W and the isotopic ratio of stem water are required by this model as input variables. At the Luancheng site, a seasonal time series of W was established by linear interpolation between weekly W measurements. Superimposed on the seasonal variation was a diurnal variation according to the diurnal composite W measured during intensive campaigns (Xiao et al., 2010; Xiao et al., 2012). The seasonal mean W was 159.7 g m^{-2} for wheat and 154.1 g m^{-2} for corn. The other input variables needed by the NSS model, the transpiration rate, canopy temperature, relative humidity in reference to canopy temperature (RH_c), and the resistance terms were determined by the S-W model outputs (Appendix A). The resistance terms were used to determine the kinetic factor for T (Lee et al. 2009).

At the Mase site, because of the lack of stem water isotope measurement, we assumed that the δ value of stem water was the same as that of the surface water. A typical value of W of 110 g m^{-2} for rice plant (Ishihara et al., 1974) was assumed for the rice growing season. Time changes in W were not considered; Xiao et al. (2012) showed that the foliage isotope enrichment is not sensitive to time variations in W.

In addition to δ_E and δ_T the transpiration isotopic submodel also calculates the isotopic composition of bulk leaf water $\delta_{L,b}$. Although not used for ET partitioning, $\delta_{L,b}$ is a useful variable to understand the non-steady state isotopic behaviors and to gage the submodel performance. To evaluate the transpiration isotopic submodel, we compared the

modeled $\delta_{L,b}$ against the measured values. Detailed information about the δ_T and $\delta_{L,b}$ equations can be found in Appendix C.

In this study, we quantify T/ET using three methods, the S-W model, a combination of eddy covariance and lysimeter measurements (for wheat only), and an isotopic partitioning approach based on the SSA and NSS δ_T estimation. Fig. 2 shows the relationships between the first and the third methods.

2.4. Performance evaluation and sensitivity analysis

Four performance measures, including root mean squares error (RMSE), index of agreement (I), bias index (BI), and coefficient of variation (R^2), were used to evaluate the model performance, as

$$RMSE = \left[\frac{1}{N}\sum_{i=1}^{N}(S_i - M_i)^2\right]^{1/2} \quad (2)$$

$$I = 1 - \frac{\sum_{i=1}^{N}(S_i - M_i)^2}{\sum_{i=1}^{N}(|S_i - \overline{M}| + |M_i - \overline{M}|)^2} \quad (3)$$

$$BI = \frac{1}{N}\sum_{i=1}^{N}(M_i - S_i) \quad (4)$$

$$R^2 = \left[\frac{\sum_{i=1}^{N}(S_i - \overline{S})(M_i - \overline{M})}{\sqrt{\sum_{i=1}^{N}(M_i - \overline{M})^2 \sum_{i=1}^{N}(M_i - \overline{M})^2}}\right]^2 \quad (5)$$

where N is total number of observations, S_i is modeled value, and M_i is observed value.

A sensitivity analysis was conducted to quantify model errors that may arise due to uncertainties in the measured input variables. The approach was proposed by Beven (1979) and Wang and Yamanaka (2014). The sensitivity coefficient (SC_j) is given by

$$SC_j = \frac{1}{N}\sum_{i=1}^{N}\frac{\partial O_{i,j}}{\partial P_{i,j}}\frac{P_{i,j}}{O_{i,j}} \quad (6)$$

where P_j is the *j*th variable in question, subscript *i* denote the *i*th observation, N is total number of observations, O is output variable, which is either the ET flux or the flux ratio T/ET. The differential $\partial O_{i,j}/\partial P_{i,j}$ is estimated as:

$$\frac{\partial O_{i,j}}{\partial P_{i,j}} = \frac{O_P^* - O_P}{P^* - P} \quad (7)$$

where O_P^* is the predicted O with a provisionally-assumed value of P, and O_P is the predicted O with the default model variable value or the measured input variable value (Beven, 1979). A positive SC_j value of 0.1 means that a 1% increase in P_j induces a 0.1% increase in O. Note that only daytime (07:00–17:00 local time) data were used for this sensitivity analysis because nighttime water vapor flux is a minor component of the daily mean flux to the atmosphere.

3. Results

3.1. Performance of the S-W model at different time scales and different sites

In general, the model has successfully simulated ET for the three ecosystems. No obvious bias is detected during the whole growing seasons. As an example, Fig. 3 shows variations of the simulated and measured hourly latent heat flux during the peak growing season (LAI close to 4) for rice, wheat and corn. The model performance statistics based on hourly values for the whole season are shown in Table 1a. The model slightly underestimates ET for rice and wheat, by 2% and 1%, respectively, and slightly overestimates ET for corn by about 1%. The daily ET means have smaller RMSEs than the hourly means (Table 1b). The seasonal mean bias errors of the whole-ecosystem latent heat flux are 4.3 W m^{-2}, −0.4 W m^{-2} and −0.8 W m^{-2} for rice, wheat and corn, respectively.

The model was further tested using the data measured at AmeriFlux sites US-NE1, US-NE2, US-NE3 and US-RO3 consisting of corn-soybean rotation. The tunable parameter (D0) in the stomatal parameterization was set to 0.35 and 0.40 for soybean and corn ecosystems, respectively (Supplementary Table S1). The S-W model reproduced the observed ET very well, with a bias within 10% and a high correlation ($R^2 > 0.87$; Supplementary Figs. S1 and S2).

3.2. Isotopic composition of canopy foliage water

A comparison of the observed and modeled isotope composition of the bulk leaf water ($\delta_{L,b}$) is given in Fig. 4. A summary of statistics is shown in Table 2. The isotope composition of the leaf water is simulated reasonably well, with R^2 equal to 0.73, I index of 0.92, BI of 0.13‰ and RMSE of 2.46‰ using SSA for wheat, and R^2 equal to 0.76 (0.82), I index of 0.92 (0.93), BI of 0.04‰ and RMSE of 2.89‰ using SSA for corn; using NSS, the R^2 is equal to 0.74, I index is 0.92, BI is −0.31‰ and RMSE is 2.63‰ for wheat, and R^2 is equal to 0.82, I index is 0.93, BI is −0.58‰ and RMSE is 2.74‰ for corn.

Similar to Xiao et al. (2012), the SSA and the NSS model produced nearly identical results for the daytime (9:00–16:00 local time) and the main discrepancy occurred in the nighttime (Fig. 4). The low sensitivity of the simulated $\delta_{L,b}$ to the SSA in the daytime is related to the short turnover time of foliage water (less than 1 h, Wang et al., 2015) and lack of the Péclet effect at the canopy scale (Xiao et al., 2010). The larger nighttime differences between the NSS and the SSA results can be partially explained by a large foliage water turnover time (greater than 200 h; Wang et al., 2015) at night. Because isotopic composition in the bulk leaf plays a major role in the isotopic exchange between the ecosystem and atmosphere, the good correlation between the simulated and observed isotopic composition in the canopy foliage suggests that our model is reasonably robust.

3.3. T/ET seasonal variations

Fig. 5 shows the seasonal variations of T/ET based on the S-W model and on the isotope approach deploying the SSA and the NSS assumption. Here, the T/ET variation displays a strong seasonal cycle, varying between 0.0–0.6 for the SW model and 0.2–1.0 for the isotope method for rice, 0.5–1.0 for the measurement, 0.6–0.9 for the SW model and 0.8–1.0 for the isotope method for wheat, and 0.2–0.7 for the SW model and 0.2–1.0 for the isotope methods for corn. According to the S-W model, T/ET for rice and corn increase almost continuously with the vegetation growth in the early growing season, and becomes relatively constant after the crops established dense foliage (LAI > 2.5). Similar trend can be found in the isotope results, although a higher T/ET ratio can be found in most of the observation days. The difference in the daily T/ET between the isotope method and the S-W numerical modeling ranges from 0 to 0.5 for rice, 0 to 0.2 for wheat and 0 to 0.4 for corn. For seasonal timescale estimation, T/ET is not sensitive to the SSA assumption (Fig. 5), although many studies have documented the impact of NSS on diurnal δ_T estimations (Lai et al., 2006; Dubbert et al., 2013; Dubbert et al., 2014b). For the whole measurement period, the S-W model results show that T/ET is 0.50, 0.84 and 0.64, and the isotopic approach shows that T/ET is 0.74, 0.93 and 0.81, for rice, wheat and corn, respectively (Table 3). The two-source model results are in better agreement than the isotopic method with the soil lysimeter and eddy covariance measurement made during the same time period for wheat (T/ET = 0.87).

3.4. Sensitivity analysis

Supplementary Table S2 summarizes the sensitivity of ET and T/ET to the measured input variables. In the case of the S-W model, RH is the

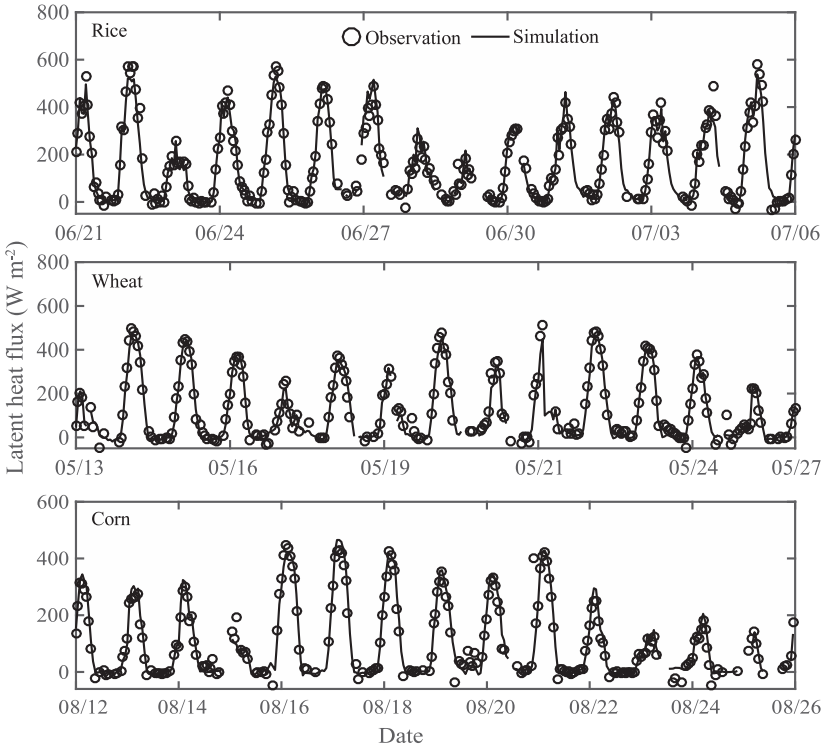

Fig. 3. Comparison of modeled and observed latent heat flux (W m^{-2}) for periods when LAI is close to 4 m^2 m^{-2}. Statistics of the model performance for the whole observation seasons are presented in Table 1.

Table 1
Statistics of the S-W model performance as measured by errors in the latent heat flux calculations at hourly (a) and daily time steps (b).

Crop	R^2	RMSE (W m^{-2})	Bias (W m^{-2})	I-index
(a)				
Rice	0.96	33.9	4.3	0.99
Wheat	0.93	42.6	−0.3	0.98
Corn	0.94	28.8	−0.5	0.99
(b)				
Rice	0.97	12.7	4.3	0.99
Wheat	0.95	14.5	−0.4	0.99
Corn	0.94	12.1	−0.8	0.98

Table 2
Statistics of the isotope model performance as measured by errors in the calculated $\delta^{18}O$ of bulk leaf water in Luancheng site. SSA indicates steady state isotopic behavior of transpiration and NSS indicates non-steady state isotopic behavior.

Crop		R^2	RMSE (‰)	Bias (‰)	I-index
Wheat	SSA	0.73	2.46	0.13	0.92
	NSS	0.74	2.63	−0.31	0.92
Corn	SSA	0.76	2.89	−0.04	0.92
	NSS	0.82	2.74	−0.58	0.93

most influential in changing ET; a 10% increase in this variable can introduce an average ET bias error of −9.2% (rice), −5.9% (wheat) and −9.1% (corn). The most influential factor for ET partitioning is net radiation (R_n) for rice, soil moisture content (θ_s) for wheat, and LAI for corn. A 10% increase in Rn, θ_s and LAI can introduce a mean relative change of 6.0%, 2.3% and 3.6% in T/ET for rice, wheat and corn, respectively.

For the isotopes approach, the most influential factors affecting T/ET are RH, δ_{ET} and δ_v for rice, wheat and corn, respectively, under both the SSA and the NSS assumption. A 10% increase in RH, δ_{ET} and δ_v

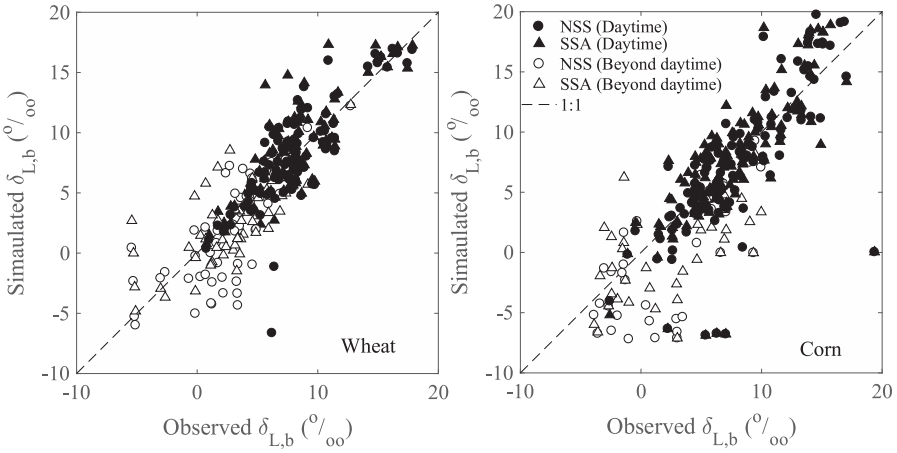

Fig. 4. Comparison of the simulated and measured oxygen isotopic composition of bulk leaf water ($\delta_{L,b}$). Statistics of the model performance are presented in Table 2. Daytime periods are 9:00–16:00 local time.

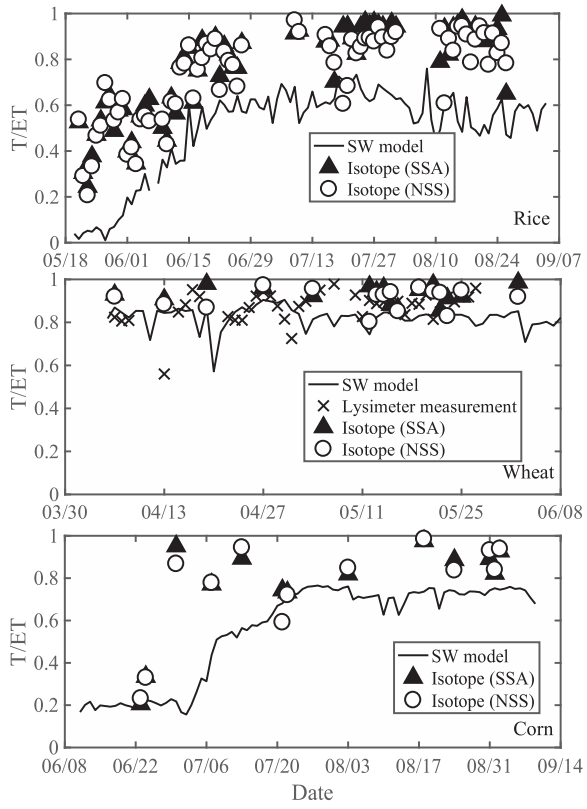

Fig. 5. Seasonal variations of T/ET determined by the isotope-based method (both SSA and NSS) for midday periods (11:00–15:00) and the daily T/ET determined by the S-W two-source model and the lysimeter / eddy covariance method.

Table 3
Comparison of ET-weighted T/ET for the whole observation periods using three different methods.

Crop	S-W model	Isotope		Lysimeter / eddy covariance measurement
		SSA	NSS	
Rice	0.50	0.77	0.74	–
Wheat	0.84	0.93	0.93	0.87
Corn	0.64	0.82	0.81	–

produces a relative change in T/ET by −4.8% (rice), −2.1% (wheat) and −2.5% (corn). Consequently, the estimated values of T/ET seem robust, as long as errors in the measured variables are bounded to 10% of the reported values. We do not expect the measurement errors in RH, δ_v and other micrometeorological variables to exceed this threshold. However, as explained in Section 4.3, errors in δ_{ET} can be larger than this.

4. Discussion

4.1. Comparison with previous studies

Several isotope-enabled land-surface models have been developed to simulate ecosystem processes related to the hydrologic cycle. Xiao et al. (2010) developed a big leaf model to simulate ET and isotopic water pools and fluxes, showing good performance (RMSE of 57 W m^{-2} for latent heat flux and 2.9‰ for $\delta_{L,b}$) for a soybean ecosystem. Their simulation was restricted to the period when the canopy was fully closed (LAI > 2), due to the neglect of soil evaporation in their model. Our model treats T and E and their isotope compositions separately. Under conditions of low LAI (< 2), the RMSE of our model is 28.8 W m^{-2} for latent heat flux and 1.97‰ (2.92‰) for NSS (SSA) for $\delta_{L,b}$ for the corn experiment; these errors are comparable to those under high LAI (> 2) conditions: the RMSE is 28.0 W m^{-2} for the latent heat flux and 2.34‰ (2.40‰) for NSS (SSA) $\delta_{L,b}$. The consistent results suggest that our model is suitable for simulating the seasonal water vapor fluxes and their isotopic variations.

Wang et al. (2015) have developed a two-source model called Iso-SPAC for partitioning evapotranspiration, with RMSEs of 37.2 W m^{-2} and 1.69‰ for the latent heat flux and $\delta_{L,b}$, respectively, for a grassland ecosystem. Iso-SPAC is based on a bulk transfer method and treats the energy balance of both vegetative canopy and at the ground. The Newton–Raphson (NR) iteration scheme is used to solve the canopy temperature and the subtract temperature (Wang et al., 2015). A further application of this model was conducted in an arid artificial oasis cropland ecosystem with high-frequency water vapor isotope measurements (Wang et al., 2016). However, the uncertainties become larger there, with RMSEs of 45.9 W m^{-2} for the latent heat flux and 4.65‰ for $\delta_{L,b}$, suggesting that some of the model parameters need further tuning to improve the model's generality. The National Centre for Atmospheric Research (NCAR) stable isotope-enabled Land Surface Model (ISOLSM) has also be used to simulate ET and its isotopic components (Riley et al., 2003; Cai et al., 2015). In Cai et al. (2015), the ISOLSM model is restricted mostly to a dry period between January 16 and 25, 2011, with an RMSE of 58.1 W m^{-2} for the latent heat flux. (The RMSE increases to 88.9 W m^{-2} for a wet period for a mixed natural eucalyptus forest.). In our study, the RMSE of the latent heat flux is 42.6 W m^{-2} for the wheat season and 28.8 W m^{-2} for the rice season (Table 1). The ISOLSM uses a two-leaf (sunlit and shaded) formulation for canopy processes. Our results indicate that the simpler one-leaf formulation actually works better, at least for the simulation of water vapor flux.

The T/ET ratio based on the S-W model compares favorably with those reported in the literature for cropland ecosystems. Our estimated full growing season T/ET for rice (0.50) is lower than for flooded wheat (0.67–0.75) reported by Balwinder-Singh et al. (2011) on the basis of microlysimeter measurements in Punjab, India. By coupling a land-surface and a crop growth model, Maruyama and Kuwagata (2010) showed that T/ET is 0.45 during a rice growth period in Tsukuba, Japan. According to weighting lysimeter and micro-lysimeter measurements made by Zhang et al. (2013), transpiration fraction during the full crop season is generally between 0.64 and 0.95 for a full wheat season consisting of mature and immature periods, and between 0.65 and 0.94 for a summer maize, with a whole season means of 0.72 and 0.60, respectively, for a winter-wheat and summer maize rotation cropland in North China Plain. Xu et al. (2016) partitioned ET via a two-source variational data assimilation system, showing a dominant contribution from T to the total ET (T/ET > 0.8) for a summer corn field. Soil lysimeter and whole-canopy lysimeter measurements published by Liu et al. (2002) indicate that canopy transpiration comprises 0.79 and 0.70 of the total evapotranspiration for a mature wheat and summer corn system, respectively, in the Luancheng site; for comparison, the T/ET ratio in our study is 0.84 for mature wheat growth phase and 0.64 for the full season of the corn growth phase.

Our isotope-based T/ET, which shows that T/ET is 0.74, 0.93 and 0.81 during the measurement period for rice, wheat and corn, respectively, is generally consistent with other isotopic studies. Wang and Yakir (2000) reported a value of 0.96 to 0.98 for a mature wheat field with a dense canopy. Wen et al. (2016) found that the relative contribution of daily T to ET ranges from 0.71 to 0.96 with a mean of 0.87 ± 0.05 for the growing season of a corn crop. Zhang et al. (2011) showed T varies from 60% to 83% of the total ET during a winter wheat season in North China Plain.

4.2. Factors controlling T/ET

Our S-W model results confirm that T/ET is controlled by LAI at the seasonal timescale (Hu et al., 2009; Good et al., 2014; Wang and

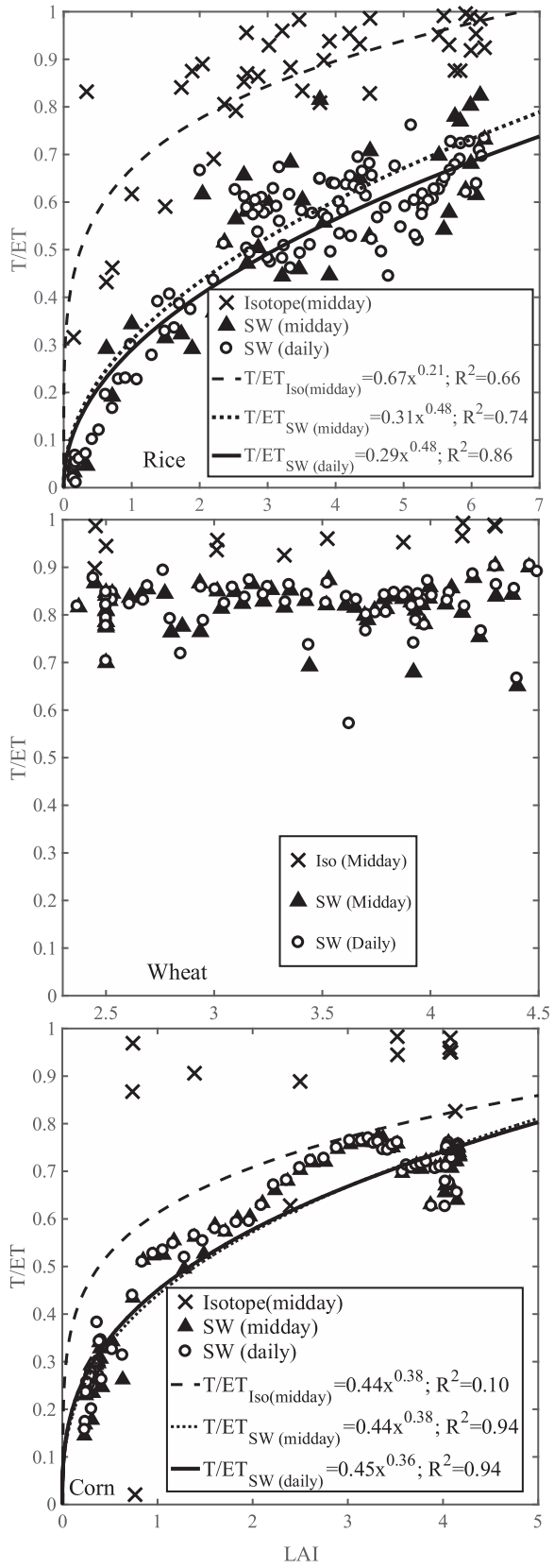

Fig. 6. Relationships between T/ET and LAI. Lines represent best fit regressions indicated.

Yamanaka, 2014; Wei et al., 2015; Berkelhammer et al., 2016). The day-to-day variations of T/ET for rice and corn are primarily controlled by LAI through its regulation of canopy radiation interception and canopy resistance; this relationship can be described with power functions (Fig. 6). For low LAI conditions (LAI ≤ 2.5), the T/ET ratio increases rapidly with increasing LAI. At higher LAI values (LAI > 2.5), even though LAI increases rapidly with time (Fig. 1), the ratio become less sensitive to LAI increase (Figs. 5 and 6). The standard deviation of T/ET for LAI ≤ 2.5 is 0.17, 0.18 for rice and corn, while for 2.5 < LAI < 6, it decreases to 0.07, 0.04, 0.03 for rice, wheat and corn, respectively. This suggests processes controlling T and E may be coupled in ways to maintain a stable T/ET ratio. The low LAI sensitivity under high LAI conditions is confirmed by soil lysimeter and eddy covariance measurements in the wheat ecosystem (Fig. 6). Some of the day-to-day variations in T/ET may have been influenced by weather fluctuations (Fig. 5), but the strong correlation between T/ET and LAI (R^2 of 0.86 for rice and 0.94 for corn) implies that the role of weather is minor in comparison to that of vegetation density. It is noted that the values of T/ET for wheat reported in Fig. 6 start at LAI > 2.4 due to lack of observations before that.

A recent meta-analysis reveals that among the 6 major global vegetation types, the T/ET versus LAI relationship of agricultural crops shows the largest spread (Wei et al., 2017). In an effort to understand the underlying causes of the spread, here we compare the monthly T/ET predicted by the S-W model with the regression result based on the global crop synthesis dataset of Wei et al. (2017) (Fig. 7). The T/ET values for corn and rice are lower than the global mean, and those for wheat and the Ameriflux sites follow closely the global trend line. All the data are within the 95% confidence bound of the global regression result.

Soil moisture may exert some influence on T/ET. In the case of rice, there was no soil moisture stress, meaning that soil moisture content was set to 100% of the field capacity. In the case of wheat, which has the same photosynthetic mode (C3) as rice, daily soil moisture varied between 0.20 and 0.34 (volume fraction), with an average of 0.27 during the growing season. The daily soil moisture for corn varied between 0.26 and 0.38 with an average of 0.31. The opposite order between T/ET (wheat > corn > rice) and soil moisture (wheat < corn < rice) under the same LAI condition indicates increasing soil moisture may reduce T/ET via increasing soil E. Other authors have also emphasized the role of soil water content in controlling T/ET (Hu et al. 2009; Liu et al., 2002). The water used for plant transpiration comes from the whole root zone, while the soil evaporation is controlled by top-soil moisture. Taking the example of wheat, the main depths of root water uptake are from 0 to 40 cm depths, while soil evaporation is controlled by soil moisture at the depth less than 20 cm (Zhang et al., 2011). Under dry conditions, although the moisture in the

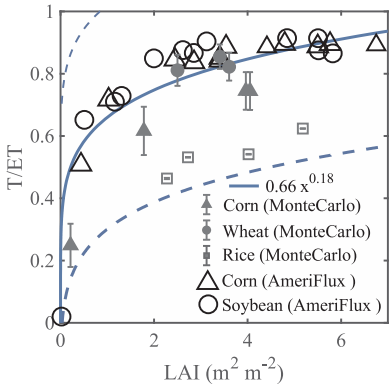

Fig. 7. Monthly T/ET predicted by the S-W model as a function LAI. The solid line represents the trend of a global crop data with the 95% confidence bound indicated by the dashed lines. Error bars are ± 1 standard deviation of Monte Carlo ensemble members.

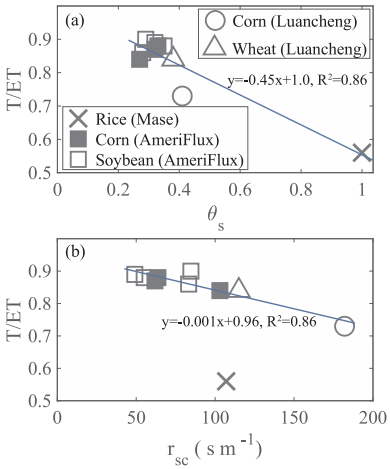

Fig. 8. Relationship between site mean T/ET and topsoil (0–20 cm depth) moisture content (volume fraction; a) and canopy resistance (b). Lines are linear regression with regression statistics noted. The data point for rice is excluded from the regression in panel (b).

root zone can meet the requirement for transpiration, soil evaporation may encounter a large surface resistance in the top soil layer, thus having the tendency to reduce E and increase T/ET. This is generally consistent with the concept proposed by Maxwell and Condon (2016), who suggests subsurface water plays a substantial role in the partitioning of evapotranspiration, and is also in agreement with the model sensitivity of wheat T/ET to soil moisture (Supplementary Table S2).

The moisture content θ_s in the top soil layer (0–20 cm depth) can explain some of the variations of the site-mean T/ET among the 10 sites (Fig. 8a). Here the mean T/ET was calculated for the period with LAI greater than 2 to minimize the effect of LAI since the model results show that T/ET becomes insensitive to LAI beyond this threshold value (Figs. 6 and 7). It is noted that use of the soil moisture at this depth here is for convenience because of data availability, but it does not imply that T/ET is controlled only by soil moisture in this soil layer. However, soil moisture cannot fully explain why T/ET at the Luancheng corn site (0.73) is much lower than the mean T/ET at the Ameriflux corn sites (US-NE1, US-NE2 and US-NE3, 0.86). The soil moisture at Luancheng corn is about 0.1 $m^3 m^{-3}$ (or a relative amount of 25%) lower than that at the Ameriflux corn sites. According to the moisture sensitivity analysis for corn (Supplementary Table S1), a reduction of soil moisture by 25% can only increase T/ET by about 0.02. On the other hand, the T/ET spread among the dryland crops is much better explained if the canopy resistance is used as an independent variable, but the flooded rice is now an outlier (Fig. 8b). Although no independent measurement is available to evaluate the S-W modeled canopy resistance, these results suggest that future studies on cropland T/ET should pay attention to plant stomatal behaviors in addition to soil moisture control. Fig. 8b also suggests that crops with saturated soil moisture, such as flooded rice, should be analyzed separately from dryland crops.

4.3. Discrepancy between isotope and non-isotope approaches

Our results demonstrate appreciable differences between the isotope and the two non-isotope flux partitioning approaches. Both the isotope and the S-W model show a nonlinear dependence of T/ET on LAI for rice and corn, but the isotope results give a higher proportion of transpiration for all the three ecosystems under the same LAI (Fig. 6). Discrepancies of this kind have also been reported by Berkelhammer et al. (2016), Schlesinger and Jasechko (2014), and Sutanto et al. (2014). These methodological differences can be largely explained by several sources of uncertainties related to the eddy covariance and stable isotope measurements and the S-W model. Uncertainties in the model input variables (Table S2) do not seem large enough to explain the biases between the two methods.

Recent isotope-based with multi-time scale synthetic studies of grass, crop and shrubland ecosystems have shown that T generally contributes more than 70% to the ET, which is about 20% higher than non-isotope based studies (Sutanto et al., 2014). A number of possible explanations for the discrepancy have been offered (Schlesinger and Jasechko, 2014; Sutanto et al., 2014), including 1) measurement errors among different techniques, 2) violation of the assumptions underlying in the methods in field conditions (such as those involved in the Keeling plot method in isotope-based studies), 3) different footprints between these approaches and the measured variables and 4) heterogeneity of field conditions. In the following we discuss some of these possibilities in the context of the methologies and measurements deployed in this study.

4.4. Mismatch in spatial and temporal scales

The model simulations rely on atmospheric measurements whose footprints are on the order of several hectares. In comparison, the isotope end members δ_E and δ_T were determined with spot measurements of isotopic compositions of individual soil/water and plant samples. To minimize the error caused by this mismatch in footprint, spatial replicates were used to obtain the mean δ_E and δ_T values. In the rice experiment, the isotopic composition of surface water was the mean value of 16 spatial replicates spread out over an area of roughly 500 m radius in the eddy flux footprint, with a standard deviation of about 5‰ in early June with low LAI and about 1‰ in August with high LAI. At the Luancheng site, the isotopic compositions of stem water and soil water were means of four spatial replicates in the dominant flux footprint and about 20 m apart from each other, with typical standard deviations of 0.2 and 0.1‰, respectively. A Monte Carlo analysis reveals that the resulting uncertainty in the seasonal mean T/ET from the isotope method (one standard deviation of 1000 ensemble members) is 0.73 ± 0.05 for rice, 0.92 ± 0.01 for wheat and 0.82 ± 0.01for corn. Footprint mismatch can introduce random errors to T/ET but does not seem to be the cause of systematic difference between the isotope method and the model.

Some of the discrepancy may also result from a mismatch in temporal scale. The isotope-based method is usually applied under high latent heat flux conditions in midday hours (Wang et al., 2013), and does not account for the evaporation that occurs at night, thus having the potential to result in an overestimation of T/ET. However, according to the S-W model calculations, the difference in T/ET between the midday (11:00–15:00 local time) and the daily time scale is not large, with an average of about 0.02 (Fig. 5).

4.5. Errors in isotope end members

Errors inherent in the determination of δ_E, δ_T, and δ_{ET} should be considered. Under the SSA, the measurement uncertainty in the xylem isotopic composition (and hence δ_T) is about 0.1–0.2 ‰. The resulting uncertainty in the full growing season T/ET is about ± 0.005 for corn and wheat. The difference in δ_T between the NSS and SSA calculations (NSS value minus SSA value) is on average 0.5‰ for rice, 0.1‰ for wheat and 0.3‰ for corn during the midday periods (11:00–15:00), and the resulting difference in T/ET is −0.03, −0.003 and −0.01 for rice, wheat and corn, respectively between the two calculations (NSS value minus SSA), suggesting that uncertainties δ_T associated with measurement errors or non-steady state isotopic behaviors is not a large source of bias error.

At the rice site, δ_{ET} was determined by the Keeling plot method. The Keeling plot assumes that the vapor isotopic ratio at our site is a mixture of contributions of water vapor from the free atmosphere and from local evapotranspiration and that within each hourly observation period, the isotopic compositions of both vapor sources are constant. With these

assumptions, the isotopic signature of evapotranspiration can be calculated as the y-intercept of a linear regression of the vapor delta value versus the inverse of the water vapor mixing ratio (Keeling, 1958). Although the Keeling plot approach is robust when applied to high temporal resolution data (Good et al., 2012), the assumptions underlying this method may not have been met perfectly in field conditions (Wei et al., 2015). Using the 1-Hz vapor isotopic data obtained by Wen et al. (2016) for an irrigated corn crop in western China, we compared the δ_{ET} derived from the Keeling plot approach with the δ_{ET} measured by the flux-gradient method. The flux-gradient method does not invoke the assumptions involved in the Keeling plot analysis, so it is likely more accurate. We found that during the midday periods, the two methods are highly correlated, but the Keeling method is biased low by 2.2‰ when compared with the flux gradient method (Supplementary Fig. S3). Assuming the same bias for the Mase site, the growing season mean T/ET would decrease from 0.74 to 0.65, bringing the isotope estimate to a closer agreement with the result produced by the S-W model (0.50).

A laboratory test shows that the δ_{ET} derived from the flux-gradient measurement using the type of analyzer deployed at Luancheng has a random error of 0.30‰ (Wen et al., 2012) and a systematic low bias of 0.33‰ (Lee et al., 2007). According to Huang and Wen (2014), the random error increases significantly under field conditions, to an average of 4.6‰ for an oasis crop ecosystem, while Hu et al. (2014) found that the random error is about 7.9‰ for a temperate grassland under low evapotranspiration conditions. A random error of 4.6‰ in δ_{ET} would result in a relative uncertainty of 43%, 31%, 32% for T/ET for the rice paddy, wheat and corn, respectively. Such an error range would be a problem for understanding day-to-day fluctuations but should not cause a systematic bias in the seasonal mean T/ET. The relative bias error in T/ET arising from a low bias error of 0.3‰ in δ_{ET} is less than 2%.

With regard to $\delta_{E,}$ potential errors can result from 1) kinetic fractionation parameterization (Dubbert et al., 2013), 2) temporal interpolation of substrate δ (Rothfuss et al., 2013), and 3) evaporation water source in the case of the dryland systems (Dubbert et al., 2013; Werner and Dubbert, 2016). Until now, there is still no agreement on the estimation of the kinetic fractionation factor ε_k in the C-G model. At the Mase site, the ε_k value (21‰) comes from a chamber evaporation experiment (Kim and Lee, 2011). The same experiment also reveals that the interfacial surface water undergoing evaporation is isotopically 7.5–8.9‰ more enriched than the bulk water below the surface. If an 8.9‰ interfacial enrichment was assumed for the water in the rice field, the T/ET for the full rice season would decrease from 0.74 to 0.65 and would improve the comparison with the S-W model (T/ET = 0.50). Alternatively, if we assume that δ_{ET} is biased low by 2.2‰ and all other errors occur in $\varepsilon_{k,}$ reducing the seasonal mean T/ET to 0.50 will require a value of 43‰ for ε_k associated with the evaporation of the standing water in the paddy field, which exceeds the molecular limit of 32‰ and is therefore unacceptable. It appears that at the high T/ET bias of the isotopic method at the Mase site is a result of biases in δ_{ET} and surficial enrichment of the paddy water below the canopy.

In the case of wheat and corn, it is difficult to determine which soil layer δ should be used for the isotopic composition of soil water undergoing evaporation, and yet this variable is a critical C-G model input. Currently, δ_E was calculated with the soil water δ measured at the 5 cm depth. Hu et al. (2014) showed that in a grass field, the difference of midday δ between 5 cm and 15 cm depths is relatively small (2.8‰) on days with high soil water content, but become larger (7.7‰) on days with low soil moisture. At the Luancheng site, the vertical variations in the soil water delta value are 1.75‰ on average among the 5 cm, 15 cm and 25 cm soil depths. A model simulation suggests that the depth with the most enriched isotopic signal is found at the soil evaporation front (Mathieu and Bariac,1996). A theoretical estimate of δ at the soil evaporation front is about 1–6‰ more enriched as compared to the values measured in the top 1 cm of the soil (Rothfuss et al., 2013). Dubbert et al. (2013) also found a strong increase in δ at the top of the soil profile with the most enriched δ values at the 0–5 cm soil depth. It is possible that the δ value measured at the 5 cm depth was an underestimate of the δ value of water at the soil evaporation front at the Luancheng site. To match the seasonal mean T/ET ratio produced by the S-W model, a 7.9‰ and 13.0‰ enrichment of soil δ above the δ value observed at the 5 cm depth is required for wheat and corn, respectively, under the SSA. Alternatively, this extra enrichment leads to the hypothesis that evaporative enrichment is confined to a thin film of water surrounding soil particles whose isotopic composition is much higher than the measured value of the bulk soil water. In this regard, the process would be similar to that involved in evaporation in the plant leaf where the water undergoing evaporation is much more enriched than the bulk leaf water.

4.6. Errors in eddy covariance flux

The discrepancy between the isotope and the non-isotope approach (eddy covariance and lysimeter combination) cannot be fully explained by the isotopic measurements errors. Based on the principle of energy budget conservation, the evapotranspiration measured by the eddy covariance instrument had a bias error of about 3%, 16% and 22% for wheat, corn and rice, respectively, if we assumed the available energy and the Bowen ratio were accurately measured. This underestimation introduced some uncertainty for ET partitioning using the eddy covariance –lysimeter combination. In this combination approach, the T flux was computed as the difference between the ET flux observed with eddy covariance and E flux observed with the lysimeters. If we used the observed ET before adjustment for energy balance, the seasonal T/ET was 0.87 for wheat (Table 3). If we adjusted the eddy-covariance ET by forcing energy balance closure, the seasonal T/ET of wheat would increase slightly to 0.88, which is closer to that derived from isotope approach. The energy balance adjustment would have a larger effect for rice and corn had there been lysimeter measurements during these crop seasons. This point can be demonstrated by a hypothetical analysis. If we assume that the modeled E is an accurate representation of evaporation, we can compute T as the difference between the observed ET and the modeled E. The seasonal T/ET is 0.34, 0.83 and 0.59 for rice, wheat and corn, respectively, before energy balance adjustment, and increases to 0.49, 0.84 and 0.64 for rice, wheat and corn, respectively, if the observed ET is adjusted using the Bowen ratio method.

4.7. Errors in the S-W model

The S-W model was calibrated against the ET measured with eddy covariance and adjusted for energy balance, by tuning one parameter in the canopy resistance parameterization (the vapor pressure deficit constant D0). This tuning ensured that the total water vapor flux (Figs. 3, S2 and S3) and the canopy resistance were unbiased. No tuning was made to three other parameters that may affect the ET partitioning, namely the light extinction coefficient used to divide the total net radiation into the canopy and the substrate components (Eq. A18) and the two empirical coefficients in the soil surface resistance parameterization (Eq. A11). The Monte Carlo analysis suggests that the error in T/ET associated with uncertainties in these parameters is about 0.1 (one standard deviation of 1000 ensemble members) for wheat and corn and is negligible for rice (Fig. 7). In other words, the isotopic T/ET for wheat is within the error range of the model, but those for corn and rice are not.

The model error for rice can be omitted because the surface resistance parameterization was avoided due to the saturation condition. The result supports the above conclusion, that the high T/ET bias of the isotopic method at the Mase site is most likely the result of biases in δ_{ET} and surficial enrichment of the paddy water below the canopy.

5. Conclusions

The two-source model presented in this study shows good agreements with observed isotope composition in the bulk leaf water and with the ET flux. The agreement of transpiration fraction T/ET calculated by the two-source model (0.83) for the wheat growing season and the T/ET based on soil lysimeter and eddy covariance measurements (0.87), highlights the robustness of the two-source model for ET partitioning. On the other hand, the transpiration fraction T/ET estimated by the isotope method is higher than that obtained with the two-source model for all the three crops (rice, wheat and corn). A Monte Carlo analysis shows that the difference between the two methods is larger than the model uncertainty for rice and corn. One potential cause of the higher T/ET for rice via the isotopic method is that the interfacial surface water undergoing evaporation under the canopy may have been much more enriched than the measured delta value of the bulk water.

The model-estimated T/ET varies from 0 to 1, with a near continuous increase over time in the early growing season when LAI was less than 2.5 and then convergence towards a stable value beyond LAI of 2.5. The seasonal change in T/ET is well described by a function of LAI, implying that LAI was a first-order factor affecting ET partitioning. The isotope-based results also reveal a dependence on LAI. The dependence of T/ET on LAI is a well-known relationship and is useful for benchmarking the isotope method. The two-source model calculations made for 7 Ameriflux crop sites reveal that this relationship is sensitive to site soil moisture availability and canopy resistance.

The current two-source model is an improvement over previous two-source models, most of which are based on the Jarvis-Stewart stomatal empirical parameters. Our model is parameterized according to plant physiological constraints and directly links the terrestrial water flux with the carbon flux. The fact that only one parameter requires tuning makes our model more versatile than some other models. The model code is available at the open-source platform https://github.com/zhongwangwei/SiLSM_v3.

Acknowledgements

The authors would like to thank Kei Yoshimura and Keisuke Ono for sharing their data. This work was supported by the U.S. National Science Foundation (Grant AGS-1520684) and the National Natural Science Foundation of China (Grants 41475141, 41505005 and 31100359). We acknowledge the following AmeriFlux sites for their data records: US-Ne1, US-Ne2, US-Ne3 and US-RO3. All the data used in this study are available on request from the corresponding author (zhongwang.wei@yale.edu).

Appendix A. The two-source evapotranspiration model

The evapotranspiration (ET) in the two-source model is partitioned into two components, canopy transpiration (T) and soil evaporation (E), as:

$$ET = E + T = \omega_c PM_c + \omega_s PM_s \tag{A1}$$

$$PM_c = \frac{\Delta A + (\rho C_p D - \Delta r_{ac} A_s)/(r_{aa} + r_{ac})}{\Delta + \gamma [1 + r_{sc}/(r_{aa} + r_{ac})]} \tag{A2}$$

$$PM_s = \frac{\Delta A + (\rho C_p D - \Delta r_{as} (A - A_s))/(r_{aa} + r_{as})}{\Delta + \gamma [1 + r_{ss}/(r_{aa} + r_{as})]} \tag{A3}$$

$$\omega_c = \frac{1}{1 + R_c R_a/[R_s (R_c + R_a)]} \tag{A4}$$

$$\omega_s = \frac{1}{1 + R_s R_a/[R_c (R_s + R_a)]} \tag{A5}$$

$$R_s = (\Delta + \gamma) r_{as} + \gamma r_{ss} \tag{A6}$$

$$R_c = (\Delta + \gamma) r_{ac} + \gamma r_{sc} \tag{A7}$$

$$R_a = (\Delta + \gamma) r_{aa} \tag{A8}$$

where ω is a weighting factor, PM is the term similar to those in Penman–Monteith model, subscript s and c represent soil and canopy component, respectively, Δ is the slope of the saturation vapor pressure versus temperature (kPa K^{-1}). $\rho$is air density (kg m^{-3}), C_P is the specific heat of dry air at constant pressure (J kg^{-1} K^{-1}), γ is the psychrometric constant (kPa K^{-1}), D is vapor pressure deficit (kPa), r_{sc} is canopy resistance (s m^{-1}), r_{ss} is soil surface resistance (s m^{-1}), r_{ac} is canopy boundary layer resistance (s m^{-1}), r_{as} is soil boundary layer resistance between the soil surface and the canopy layer (s m^{-1}), and r_{aa} is aerodynamic resistance between the canopy source and a reference height (s m^{-1}). The calculation procedure of the r_{sc} is given in Section S2. Additionally, A and A_s are the total available energy and available energy for the soil surface (W m^{-2}),

$$A = R_n - G \tag{A9}$$

$$A_s = R_{ns} - G \tag{A10}$$

The radiation reaching the soil surface is calculated using Beer's law (e.g. Ross, 1981).

$$R_{ns} = R_n \exp(-k_r LAI) \tag{A11}$$

where R_n and R_{ns} are net radiation above the canopy and at the soil surface, respectively (W m^{-2}), and G is the soil heat flux (W m^{-2}). The canopy extinction coefficient of net radiation (k_r) is assumed as 0.6.

The aerodynamic resistances r_{as} and r_{aa} are calculated by integrating the eddy diffusion coefficients from the soil surface to the level of the preferred sink of momentum in the canopy, and from there to the reference height (Shuttleworth and Gurney, 1990),

$$r^{aa} = \frac{1}{k u_*} \ln\left(\frac{z_m - d_0}{h_c - d_0}\right) + \frac{h_c}{\kappa_m K_h}\left\{\exp\left[\kappa_m\left(1 - \frac{d_0 + z_0}{h_c}\right)\right] - 1\right\} \tag{A12}$$

$$r^{as} = \frac{h_c \exp(\kappa_m)}{\kappa_m K_h}\left\{\exp\left(\frac{-\kappa_m z^{0s}}{h_c}\right) - \exp\left[-\kappa_m\left(\frac{d_0 + z_0}{h_c}\right)\right]\right\} \tag{A13}$$

where k = 0.4 is the von Karman constant, z_m is the reference height of measurement (m), u_* is friction velocity (m s^{-1}), $d_0 = 1.1h_c \ln(1 + X^{1/4})$ is the zero-plane displacement (m), z_0 is the roughness lengths governing the transfer of momentum (m)

$$z_0 = \begin{cases} z_{0s} + 0.3h_c X^{1/2} & 0 < X < 0.2 \\ 0.3h_c(1 - d_0/h_c) & 0.2 < X < 1.5 \end{cases} \tag{A14}$$

z_{0s} is the effective roughness length of the soil substrate (m), $X = C_d LAI$, C_d is the drag coefficient, h_c is vegetation high (m), $\kappa_m = 2.5$ is the extinction coefficient of the eddy diffusion (Brutsaert, 1982) and K_h is the eddy diffusion coefficient at the top of the canopy

$$K_h = ku_*(h_c - d_0) \tag{A15}$$

The canopy boundary layer resistance r_{ac} (s m^{-1}) is calculated as

$$r^{ac} = \frac{r_b}{2LAI} \tag{A16}$$

$$r_b = \frac{100}{\kappa_m}\left(\frac{d_l}{u_h}\right)\Big/[1 - \exp(-\frac{\kappa_m}{2})] \tag{A17}$$

where r_b is the mean boundary layer resistance, determined from the wind speed at the top of canopy (u_h), and the characteristic leaf dimension.

The soil surface resistance, r_{ss} (s m^{-1}), is the resistance to water vapor movement from the interior to the surface of the soil, and is calculated using soil water content θ_s (m^3 m^{-3}):

$$r_{ss} = \exp(8.206 - 4.225 \times \theta_s) \tag{A18}$$

(Sellers et al., 1992).

Appendix B. The canopy resistance in the two-source model

The canopy resistance r_{sc} is solved from a plant physiological approach at the leaf scale and up-scaled to the canopy scale by an analytic formulation (Ronda et al., 2001). At the leaf scale, the CO_2 stomatal conductance is described by a photosynthesis-stomatal conductance model as

$$g_l^c = g_{\min,c} + \frac{a_1 A_g}{(C_l - \Gamma)\left(1 + \frac{D_s}{D_0}\right)} \tag{B1}$$

where A_g is the gross assimilation rate, $g_{min,c}$ is the cuticular conductance, C_l is the CO_2 concentration at the leaf surface, D_s is the vapor pressure deficit at plant level, a_1 is an empirical parameter equal to 9.1 for C3 and 6.6 for C4 plants, and D_0 is a tunable empirical parameter. Here, A_g is computed as a function of canopy temperature (Tc), photosynthetically active radiation (PAR) and the intercellular CO_2 concentration (C_i).

$$A_g = (A_m + R_d)\{1 - e^{-[\alpha PAR/(A_m + R_d)]}\} \tag{B2}$$

The primary productivity A_m is given by

$$A_m = A_{m,\max}\{1 - e^{-[g_m(C_l - \Gamma)/A_{m,\max}]}\} \tag{B3}$$

and the dark respiration R_d is calculated as

$$R_d = 0.11A_m \tag{B4}$$

where α is the light use efficiency, $A_{m,max}$ is the maximal primary productivity under high light and high CO_2 concentrations, g_m is the mesophyll conductance for CO_2, Γ is the CO_2 compensation point, which are functions of the canopy temperature. The detailed schemes for g_m, C_i and $A_{m,max}$ for C3 and C4 plants are given by Ronda et al. (2001). The canopy temperature T_c was solved from the transpiration flux predicted by the S-W model.

The effect of water stress on net photosynthesis and canopy conductance is accounted for by applying a soil-moisture dependent function to A_g:

$$A_g = A_g^* f_5(\theta) \tag{B5}$$

where A_g^* is the unstressed rate, and f_5 is given as

$$f_5(\theta) = 2\beta(\theta) - \beta^2(\theta) \tag{B6}$$

$$\beta(\theta) = \max\left[0, \min\left(1, \frac{\theta - WP}{FC - WP}\right)\right] \tag{B7}$$

where FC and WP are the soil moisture content at field capacity and at permanent wilting point, respectively (Xiao et al., 2010). The function β ranges from 1 (plants without water stress, such as rice under flooded condition) to 0 (at wilting point).

The method to scale g_l^c to canopy scale conductance g_c^c was presented in Ronda et al. (2001). Finally, because water vapor and carbon dioxide are exchanged by the same stomata but at different rates of diffusion, the canopy resistance r_{sc} is determined as $1/(1.6g_c^c)$.

Appendix C. Modeling isotopic compositions of evaporation and transpiration

Appendix C.1 Isotope composition of soil / substrate evaporation

The isotope composition of soil / substrate evaporation is calculated with the Craig-Gardon model,

$$\delta_E = \frac{\alpha_{eq}\delta_L - h^*\delta_a - \varepsilon_{eq} - (1-h^*)\varepsilon_k}{1 - h^* + (1-h^*)\varepsilon_k/1000} \quad \text{(C1)}$$

where δ_E is the isotopic composition of substrate evaporation (soil at Luancheng and standing water at Mase), δ_a is the isotopic ratio of vapor measured at the reference height, h^* is relative humidity expressed as a fraction in reference to the temperature of the sustrate and $\varepsilon_k$is the isotopic kinetic fractionation associated with substrate evaporation, $\alpha_{eq}$is the temperature-dependent equilibrium fractionation factor from liquid to vapor and is calculated as a function of the substrate temperature, and ε_{eq} = 1-α_{eq}. Different $\varepsilon_k$values were applied to the two sites to account for the fact that substrate evaporation originated from two different media (soil in Luangcheng and standing water in Mase). A constant $\varepsilon_k$value of 21 based on the chamber evaporation study of Kim and Lee (2011) was used for Mase (standing water) and the parameterization of Wen et al. (2012) for Luancheng (soil).

(C2) Isotopic compositions of leaf water and canopy transpiration

Under the steady-state assumption (SSA), the water leaving the leaf has the same isotope composition as the xylem water, so we have

$$\delta_T = \delta_x \quad \text{(C2)}$$

where δ_x is the isotopic ratio of xylem water, and δ_T is the isotopic ratio of transpiration.

The isotope composition of the leaf water undergoing phase change is calculated by inverting the Craig-Gordon model, as

$$\delta_{L,es} = \delta_x + \varepsilon_{eq} + \varepsilon_k + h^*(\delta_a - \varepsilon_k - \delta_x) \quad \text{(C3)}$$

where $\delta_{L,es}$ is the $\delta$of leaf water at the evaporating site in the leaves, h^* is relative humidity expressed as a fraction in reference to the canopy temperature, and ε_k is the canopy kinetic fractionation factor (Lee et al., 2009),

$$\varepsilon_k = \frac{21r_c + 19r_b}{r_a + r_b + r_c} \quad \text{(C4)}$$

where r_a, r_b and r_c are the aerodynamic, the boundary layer and the canopy resistance, respectively. The isotopic composition of the bulk leaf water $\delta_{L,bs}$under SSA is assumed as a weighted mean of the enriched part around the evaporation site and isotope composition of the xylem water (Roden and Ehleringer, 1999)

$$\delta_{L,bs} = f\delta_{L,es} + (1-f)\delta_x \quad \text{(C5)}$$

where f = 0.8 is the proportion of water associated with the evaporation site to the total leaf water.

In non-steady state conditions, δ_T can deviate fromδ_x. By considering temporal changes in the water content and the Péclet effect, Farquhar and Cernusak (2005) propose the following expressions

$$\delta_{L,b} = \delta_{L,bs} - \frac{\alpha_k\alpha_{eq}r_t}{w_i}\frac{1-e^{-P}}{P}\frac{d(W\times(\delta_{L,b}-\delta_x))}{dt} \quad \text{(C6)}$$

$$\delta_{L,e} = \delta_{L,es} - \frac{\alpha_k\alpha_{eq}r_t}{w_i}\frac{1-e^{-P}}{P}\frac{d(W\times(\delta_{L,e}-\delta_x))}{dt} \quad \text{(C7)}$$

where W is leaf water content (g m^{-2}), w_i is the mole fraction of water vapor in the intercellular space, P is Péclet number (dimensionless), r_t is total resistance to the diffusion of water vapor, and $\alpha_k = 1 + \varepsilon_k/1000$ is the fractionation factor for diffusion. The δ of transpiration under NSS is given by

$$\delta_T = \delta_x + \frac{\delta_{L,e} - \delta_{L,es}}{\alpha_k\alpha_{eq}(1-h^*)} \quad \text{(C8)}$$

Eqs. (C6) and (C7) were solved iteratively by finding a zero difference between the left- and right-hand sides of each equation (Xiao et al., 2010).

Appendix D. Supplementary data

Supplementary material related to this article can be found, in the online version, at doi:https://doi.org/10.1016/j.agrformet.2018.01.019.

References

Agam, N., et al., 2012. Evaporative loss from irrigated interrows in a highly advective semi-arid agricultural area. Adv. Water Resour. 50, 20–30.

Ashktorab, H., Pruitt, W.O., Pawu, K.T., George, W.V., 1989. Energy balance determinations close to the soil surface using a micro-Bowen ratio system. Agric. For. Meteorol. 46, 259–274.

Baldocchi, D.D., Meyers, P.T., 1991. Trace gas exchange above the floor of a decidious forest 1. Evaporation and CO2 efflux. J. Geophys. Res. 96, 7271–7285.

Balwinder-Singh, Eberbach, P.L., Humphreys, E., Kukal, S.S., 2011. The effect of rice straw mulch on evapotranspiration, transpiration and soil evaporation of irrigated wheat in Punjab. India Agric. Water Manag. 98, 1847–1855.

Berkelhammer, M., et al., 2016. Convergent Approaches to Determine an Ecosystem's Transpiration Fraction. Global Biogeochem Cy.

Beven, K., 1979. A sensitivity analysis of the Penman-Monteith actual evapotranspiration estimates. J. Hydrol. 44 (3), 169–190.

Blanken, P.D., et al., 1998. Turbulent flux measurements above and below the overstory of a boreal aspen forest. Bound Layer Meteorol. 89 (1), 109–140.

Boast, C.W., Robertson, T.M., 1982. A micro-lysimeter method for determining evaporation from bare soil: description and laboratory evaluation. Soil Sci. Soc. Am. J. 46, 689–696.

Brutsaert, W., 1982. Evaporation into the Atmosphere.

Cai, M.Y., et al., 2015. Stable water isotope and surface heat flux simulation using ISOLSM: Evaluation against in-situ measurements. J. Hydrol. 523, 67–78.

Cox, P.M., Huntingford, C., Harding, R.J., 1998. A canopy conductance and photosynthesis model for use in a GCM land surface scheme. J. Hydrol. 212 (1–4), 79–94.

Cox, P.M., Betts, R.A., Jones, C.D., Spall, S.A., Totterdell, I.J., 2000. Acceleration of global warming due to carbon-cycle feedbacks in a coupled climate model. Nature 408 (6809), 184–187.

Craig, H., Gordon, L.I., 1965. Deuterium and Oxygen 18 Variations in the Ocean and the Marine Atmosphere. Consiglio nazionale delle richerche, Laboratorio de geologia nucleare.

Ding, R., Kang, S., Du, T., Hao, X., Zhang, Y., 2014. Scaling up stomatal conductance from leaf to canopy using a dual-leaf model for estimating crop evapotranspiration. PloS One 9 (4), e95584.

Dubbert, M., Cuntz, M., Piayda, A., Maguás, C., Werner, C., 2013. Partitioning evapotranspiration – testing the Craig and Gordon model with field measurements of oxygen isotope ratios of evaporative fluxes. J. Hydrol. 496, 142–153.

Dubbert, M., Cuntz, M., Piayda, A., Werner, C., 2014a. Oxygen isotope signatures of

transpired water vapor: the role of isotopic non-steady-state transpiration under natural conditions. New Phytol. 203 (4), 1242–1252.
Dubbert, M., et al., 2014b. Stable oxygen isotope and flux partitioning demonstrates understory of an oak savanna contributes up to half of ecosystem carbon and water exchange. Front. Plant Sci. 5, 530.
Egea, G., Verhoef, A., Vidale, P.L., 2011. Towards an improved and more flexible representation of water stress in coupled photosynthesis-stomatal conductance models. Agric. For. Meteorol. 151 (10), 1370–1384.
Farquhar, G.D., Cernusak, L.A., 2005. On the isotopic composition of leaf water in the non-steady state. Funct. Plant Biol. 32 (4), 293.
Good, S.P., Noone, D., Bowen, G., 2015. Hydrologic connectivity constrains partitioning of global terrestrial water fluxes. Science 349 (6244), 175–177.
Good, S.P., et al., 2014. δ2H isotopic flux partitioning of evapotranspiration over a grass field following a water pulse and subsequent dry down. Water Resour. Res. 50 (2), 1410–1432.
Good, S.P., Soderberg, K., Wang, L.X., Caylor, K.K., 2012. Uncertainties in the assessment of the isotopic composition of surface fluxes: A direct comparison of techniques using laser-based water vapor isotope analyzers. J. Geophys. Res. Atmos. 117.
Henderson-Sellers, A., et al., 2006. Stable water isotope simulation by current land-surface schemes: results of iPILPS phase 1. Glob. Planet. Change 51 (1–2), 34–58.
Hu, Z., et al., 2014. Partitioning of evapotranspiration through oxygen isotopic measurements of water pools and fluxes in a temperate grassland. J. Geophys. Res. Biogeosci. 119 (3), 358–372.
Hu, Z.M., et al., 2009. Partitioning of evapotranspiration and its controls in four grassland ecosystems: application of a two-source model. Agric. For. Meteorol. 149 (9), 1410–1420.
Huang, L., Wen, X., 2014. Temporal variations of atmospheric water vaporδD andδ18O above an arid artificial oasis cropland in the Heihe River Basin. J. Geophys. Res. Atmos. 119 (19), 476 11,456-11.
Holland, S., Heitman, J.L., Howard, A., Sauer, T.J., Giese, W., Ben-Gal, A., Agam, N., Kool, D., Havlin, J., 2013. Micro-Bowen ratio system for measuring evapotranspiration in a vineyard interrow. Agric. For. Meteorol. 177, 93–100.
Ishihara, K., Ishida, Y., Ogura, T., 1974. On the diurnal variation of leaf water content on an areal basis in the rice plant. Jpn. J. Crop. Sci. 43 (1), 77–82.
Jasechko, S., et al., 2013. Terrestrial water fluxes dominated by transpiration. Nature 496 (7445), 347–350.
Kato, T., Kimura, R., Kamichika, M., 2004. Estimation of evapotranspiration, transpiration ratio and water-use efficiency from a sparse canopy using a compartment model. Agric. Water Manage. 65 (3), 173–191.
Keeling, C.D., 1958. The concentration and isotopic abundances of atmospheric carbon dioxide in rural areas. Geochim. Cosmochim. Acta 13 (4), 322–334.
Kim, K., Lee, X., 2011. Isotopic enrichment of liquid water during evaporation from water surfaces. J. Hydrol. 399 (3-–4), 364–375.
Lai, C.T., Ehleringer, J.R., Bond, B.J., U, K.T.P., 2006. Contributions of evaporation, isotopic non-steady state transpiration and atmospheric mixing on the delta O-18 of water vapour in pacific northwest coniferous forests. Plant Cell Environ. 29 (1), 77–94.
Lee, H., Smith, R., Williams, J., 2006. Water vapour O-18/O-16 isotope ratio in surface air in New England, USA. Tellus B 58 (4), 293–304.
Lee, X., et al., 2009. Canopy-scale kinetic fractionation of atmospheric carbon dioxide and water vapor isotopes. Glob. Biogeochem. Cycl. 23 (1).
Lee, X., Kim, K., Smith, R., 2007. Temporal variations of the (18)O/(16)O signal of the whole-canopy transpiration in a temperate forest. Glob. Biogeochem. Cycl. 21 (3).
Lee, X., Huang, J., Patton, E.G., 2011. A large-eddy simulation study of water vapour and carbon dioxide isotopes in the atmospheric boundary layer. Bound Layer Meteorol. 145 (1), 229–248.
Liu, C., Zhang, X., Zhang, Y., 2002. Determination of daily evaporation and evapotranspiration of winter wheat and maize by large-scale weighing lysimeter and microlysimeter. Agric For. Meteorol. 111 (2), 109–120.
Mathieu, R., Bariac, T., 1996. A numerical model for the simulation of stable isotope profiles in drying soils. J. Geophys. Res. Atmos. 101 (D7), 12685–12696.
Maruyama, A., Kuwagata, T., 2010. Coupling land surface and crop growth models to estimate the effects of changes in the growing season on energy balance and water use of rice paddies. Agric. For. Meteorol. 150 (7–8), 919–930.
Maxwell, R.M., Condon, L.E., 2016. Connections between groundwater flow and transpiration partitioning. Science 353 (6297), 377–380.
Medvigy, D., Wofsy, S.C., Munger, J.W., Moorcroft, P.R., 2010. Responses of terrestrial ecosystems and carbon budgets to current and future environmental variability. Proc. Natl. Acad. Sci. U. S. A. 107 (18), 8275–8280.
Miralles, D.G., et al., 2016. The WACMOS-ET project – part 2: evaluation of global terrestrial evaporation data sets. Hydrol. Earth Syst. Sci. 20 (2), 823–842.
Moran, M.S., Scott, R.L., Keefer, T.O., Emmerich, W.E., Hernandez, M., Nearing, G.S., Paige, G.B., Cosh, M.H., O'Neill, P.E., 2009. Partitioning evapotranspiration in semiarid grassland and shrubland ecosystems using time series of soil surface temperature. Agric. For. Meteorol. 149 (1), 59–72.
Niyogi, D., Alapaty, K., Raman, S., Chen, F., 2009. Development and evaluation of a coupled photosynthesis-based gas exchange evapotranspiration model (GEM) for mesoscale weather forecasting applications. J. Appl. Meteorol. Clim. 48 (2), 349–368.
Riley, W.J., Still, C.J., Helliker, B.R., Ribas-Carbo, M., Berry, J.A., 2003. O-18 composition of CO2 and H2O ecosystem pools and fluxes in a tallgrass prairie: simulations and comparisons to measurements. Glob. Change Biol. 9 (11), 1567–1581.
Roden, J.S., Ehleringer, J.R., 1999. Observations of hydrogen and oxygen isotopes in leaf water confirm the Craig-Gordon model under wide-ranging environmental conditions. Plant Physiol. 120 (4), 1165–1174.
Ronda, R.J., de Bruin, H.A.R., Holtslag, A.A.M., 2001. Representation of the canopy conductance in modeling the surface energy budget for low vegetation. J. Appl. Meteorol. 40 (8), 1431–1444.
Ross, J., 1981. The Radiation Regime and Architecture of Plant Stands. Junk, London, pp. 391.
Rothfuss, Y., et al., 2010. Partitioning evapotranspiration fluxes into soil evaporation and plant transpiration using water stable isotopes under controlled conditions. Hydrol. Process. 24 (22), 3177–3194.
Rothfuss, Y., Vereecken, H., Brüggemann, N., 2013. Monitoring water stable isotopic composition in soils using gas-permeable tubing and infrared laser absorption spectroscopy. Water Resour. Res. 49 (6), 3747–3755.
Raz-Yaseef, N., Yakir, D., Schiller, G., Cohen, S., 2012. Dynamics of evapotranspiration partitioning in a semi-arid forest as affected by temporal rainfall patterns. Agric. For. Meteorol. 157, 77–85.
Sakuratani, T., 1981. A heat balance method for measuring water flux in the stem of intact plants. J. Agric. Meteorol. 37, 9–17.
Sakuratani, T., 1987. Studies of evaporation from crops. II. Separate estimation of transpiration and evaporation from a soybean field without water shortage. J. Agric. Meteorol. 42, 309–317.
Schlesinger, W.H., Jasechko, S., 2014. Transpiration in the global water cycle. J. Agric. Meteorol. 189–190 (0), 115–117.
Schultz, N.M., Griffis, T.J., Lee, X., Baker, J.M., 2011. Identification and correction of spectral contamination in 2H/1H and 18O/16O measured in leaf, stem, and soil water. Rapid Commun. Mass Spectrom. 25, 3360–3368.
Sellers, P.J., Heiser, M.D., Hall, F.G., 1992. Relations between surface conductance and spectral vegetation indices at intermediate (100 m^2 to 15 km^2) length scales. J. Geophys. Res.: Atmos. 97 (D17), 19033–19059.
Sellers, P.J., et al., 1996. A revised land surface parameterization (SiB2) for atmospheric GCMs. 1. Model formulation. J. Clim. 9 (4), 676–705.
Shawcroft, R.W., Gardner, H.R., 1983. Direct evaporation from soil under a row crop canopy. Agric. Meteorol. 28, 229–238.
Shuttleworth, W.J., Gurney, R.J., 1990. The theoretical relationship between foliage temperature and canopy resistance in sparse crops. Q. J. R. Meteorol. Soc. 116 (492), 497–519.
Shuttleworth, W.J., Wallace, J.S., 1985. Evaporation from sparse crops-an energy combination theory. Q. J. R. Meteorol. Soc. 111 (469), 839–855.
Siebert, S., Döll, P., 2010. Quantifying blue and green virtual water contents in global crop production as well as potential production losses without irrigation. J. Hydrol. 384 (3–4), 198–217.
Stannard, D.I., 1993. Comparison of Penman-Monteith, Shuttleworth-Wallace, and modified Priestley-Taylor evapotranspiration models for wildland vegetation in semiarid rangeland. Water Resour. Res. 29 (5), 1379–1392.
Stannard, D.I., Weltz, M.A., 2006. Partitioning evapotranspiration in sparsely vegetated rangeland using a portable chamber. Water Resour. Res. 42 (2).
Sun, H.Y., Liu, C.M., Zhang, X.Y., Shen, Y.J., Zhang, Y.Q., 2006. Effects of irrigation on water balance, yield and WUE of winter wheat in the North China plain. Agric. Water Manage. 85 (1-2), 211–218.
Sutanto, S.J., et al., 2014. HESS opinions "a perspective on isotope versus non-isotope approaches to determine the contribution of transpiration to total evaporation". Hydrol. Earth Syst. Sci. 18 (8), 2815–2827.
Twine, T.E., et al., 2000. Correcting eddy-covariance flux underestimates over a grassland. Agric. For. Meteorol. 103 (3), 279–300.
Vörösmarty, C.J., Federer, C.A., Schloss, A.L., 1998. Potential evaporation functions compared on US watersheds: possible implications for global-scale water balance and terrestrial ecosystem modeling. J. Hydrol. 207 (3), 147–169.
Walker, G.K., 1984. Evaporation from wet soil surfaces beneath plant canopies. Agric. For. Meteorol. 33, 259–264.
Wang, L., et al., 2013. The effect of warming on grassland evapotranspiration partitioning using laser-based isotope monitoring techniques. Geochim. Cosmochim. Acta 111, 28–38.
Wang, P., et al., 2016. Numerical modeling the isotopic composition of evapotranspiration in an arid artificial oasis cropland ecosystem with high-frequency water vapor isotope measurement. Agric. For. Meteorol. 230–231 (December), 79–88. http://dx.doi.org/10.1016/j.agrformet.2015.12.063. Part of special issue: Oasis-desert system.
Wang, P., Yamanaka, T., 2014. Application of a two- source model for partitioning evapotranspiration and assessing its controls in temperate grasslands in central Japan. Ecohydrology 7 (2), 345–353.
Wang, P., Yamanaka, T., Li, X.Y., Wei, Z.W., 2015. Partitioning evapotranspiration in a temperate grassland ecosystem: numerical modeling with isotopic tracers. Agric. For. Meteorol. 208 (0), 16–31.
Wang, X.F., Yakir, D., 2000. Using stable isotopes of water in evapotranspiration studies. Hydrol. Process. 14 (8), 1407–1421.
Wei, Z., et al., 2015. Partitioning of evapotranspiration using high-frequency water vapor isotopic measurement over a rice paddy field. Water Resour. Res. 51 (5), 3716–3729.
Wei, Z., et al., 2016. Understanding the variability of water isotopologues in near-surface atmospheric moisture over a humid subtropical rice paddy in Tsukuba, Japan. J. Hydrol 533, 91–102.
Wei, Z., et al., 2017. Revisiting the contribution of transpiration to global terrestrial evapotranspiration. Geophys. Res. Lett. 44 (6), 2792–2801.
Wen, X., Yang, B., Sun, X., Lee, X., 2016. Evapotranspiration partitioning through in-situ oxygen isotope measurements in an oasis cropland. Agric. For. Meteorol. 230-231, 89–96.
Wen, X.F., et al., 2012. Dew water isotopic ratios and their relationships to ecosystem water pools and fluxes in a cropland and a grassland in China. Oecologia 168 (2), 549–561.
Werner, C., et al., 2012. Progress and challenges in using stable isotopes to trace plant carbon and water relations across scales. Biogeosciences 9 (8), 3083–3111.
Werner, C., Dubbert, M., 2016. Resolving rapid dynamics of soil–plant–atmosphere

interactions. New Phytol. 210, 767–769.
Williams, D.G., et al., 2004. Evapotranspiration components determined by stable isotope, sap flow and eddy covariance techniques. Agric. For. Meteorol. 125 (3–4), 241–258.
Wilson, K.B., Hanson, P.J., Mulholland, P.J., Baldocchi, D.D., Wullschleger, S.D., 2001. A comparison of methods for determining forest evapotranspiration and its components: sap-flow, soil water budget, eddy covariance and catchment water balance. Agric. For. Meteorol. 106 (2), 153–168.
Xiao, W., et al., 2010. A modeling investigation of canopy-air oxygen isotopic exchange of water vapor and carbon dioxide in a soybean field. J. Geophys. Res. 115 (G1).
Xiao, W., Lee, X.H., Wen, X.F., Sun, X.M., Zhang, S.C., 2012. Modeling biophysical controls on canopy foliage water 18O enrichment in wheat and corn. Glob. Change Biol. 18 (5), 1769–1780.
Xu, T., Bateni, S.M., Margulis, S.A., Song, L., Liu, S., Xu, Z., 2016. Partitioning evapotranspiration into soil evaporation and canopy transpiration via a two-source variational data assimilation system. J. Hydrometeorol. 17 (9), 2353–2370.
Yakir, D., Sternberg, L.D.L., 2000. The use of stable isotopes to study ecosystem gas exchange. Oecologia 123 (3), 297–311.
Yepez, E.A., et al., 2005. Dynamics of transpiration and evaporation following a moisture pulse in semiarid grassland: a chamber-based isotope method for partitioning flux components. Agric. For. Meteorol. 132 (3–4), 359–376.
Yoshimura, K., Kanamitsu, M., Noone, D., Oki, T., 2008. Historical isotope simulation using reanalysis atmospheric data. J. Geophys. Res. Atmos. 113 (D19), D19108.
Zeggaf, A.T., Takeuchi, S., Dehghanisanij, H., Anyoji, H., Yano, T., 2008. A Bowen ratio technique for partitioning energy fluxes between maize transpiration and soil surface evaporation. Agron. J. 100, 988–996.
Zhang, B., et al., 2013. The dual crop coefficient approach to estimate and partitioning evapotranspiration of the winter wheat–summer maize crop sequence in North China plain. Irrig. Sci. 31 (6), 1303–1316.
Zhang, Y., Liu, C., Shen, Y., Kondoh, A., Tang, C., Tanaka, T., Shimada, J., 2002. Measurement of evapotranspiration in a winter wheat field. Hydrol. Process. 16 (14), 2805–2817.
Zhang, Y.C., Shen, Y.J., Sun, H.Y., Gates, J.B., 2011. Evapotranspiration and its partitioning in an irrigated winter wheat field: a combined isotopic and micrometeorologic approach. J. Hydrol. 408 (3–4), 203–211.